Hindawi
Mathematical Problems in Engineering
Volume 2022, Article ID 3146658, 9 pages
https://doi.org/10.1155/2022/3146658

Research Article

Performance Optimization of Helicopter Rotor in Hover Based on CFD Simulation

Chenglong Zhou,[1] Anan Xu,[2] Fang Wang,[3] Ming Chen,[3] Wei Li,[1] and Rui Yin[1]

[1]*Information Science Academy of China Electronics Technology Group Corporation, Building 4, Yard 30, Jinfu Road, Shijingshan District, Beijing 100041, China*
[2]*School of Aeronautic Science and Engineering, Beihang University, Xueyuan Road No. 37, Beijing 100191, China*
[3]*Institute of Unmanned System, Beihang University, Xueyuan Road No. 37, Beijing 100191, China*

Correspondence should be addressed to Fang Wang; buaaairforce@buaa.edu.cn

Received 7 June 2022; Accepted 13 July 2022; Published 10 August 2022

Academic Editor: Amandeep Kaur

An optimization method of helicopter rotor hovering performance is proposed, which is mainly carried out by means of CFD simulation. This method can be used to obtain the rotation speed of any blade model under the designed hovering tension through several iterations, and then, the tension, torque, power, and power load of the rotor under the rotation speed can be obtained. By comparing different blade pitch, radius, twist, and chord length, the blade parameters at the highest power load can be selected. A series of new rotor models are obtained by changing the model parameters on the basis of C-T rotor. NASA has carried out a lot of experiments on the C-T rotor model and published detailed experimental reports. The transient simulation is carried out by the embedded grid method.

1. Introduction

The aerodynamic performance of helicopter has a great impact on its overall performance, which is a key problem to be solved in engineering development. Hovering state is one of the most important flight states of a helicopter, which must be considered in the process of helicopter aerodynamic design [1].

In the past, the aerodynamic performance of the helicopter was mainly studied by experimental methods. Now, with the rapid development of computer technology, computational fluid dynamics has been paid more and more attention. The results of the experimental method are more reliable and more suitable for simple problems such as reducing fuselage resistance [2, 3]. However, the experimental method is difficult to observe the detailed characteristics of the helicopter flow field and is often time-consuming and expensive. CFD technology has been developing rapidly in the field of helicopter aerodynamic optimization due to its low cost, short time consumption, and high accuracy.

Nowadays, there are many CFD methods applied to helicopter rotor aerodynamic simulation [4, 5]. Among them, the embedded grid method [6] is the most widely used. This method is applicable to helicopter hovering, forward flight, vertical flight, near ground flight, and other complex flight states. Due to the difficulty in realizing the periodic change of pitch, the sliding grid method cannot be applied to the forward flight state of helicopter. However, it is suitable for calculating the hovering state of the helicopter and is widely used in this field. Steijl and Barakos [7] introduced the sliding mesh method and proved that this method has high precision through several examples. The adaptive mesh method [8, 9] can automatically encrypt the region with large gradient according to the preliminary calculation results, so as to improve the calculation accuracy. It is highly regarded in the field of helicopter aerodynamic simulation, and it can easily capture the wake of rotor vortex. Jameson and Mavriplis [10] adopted the multigrid method to effectively improve the computational efficiency of CFD simulation. Zhao et al. [11] developed the CLORNS code to

solve the unsteady aerodynamic flow field of helicopter rotors and achieved good results. Zhou and Chen [12] proposed a CFD balancing method for helicopter forward flight state, which has a high engineering practical value. Barakos et al. [13] used the method of Actuator Disks (AD) to calculate the rotor flow field in hovering and forward flight and captured the main vortex structure around the rotor disc well. Lyu et al. [14] put forward some improvement suggestions on the hybrid trim method based on CFD for helicopter rotor forward flight.

Generally, in order to determine the accuracy of numerical simulation results, it is necessary to compare the numerical solutions with the experimental values. Detailed test parameters of the C-T rotor selected in this paper at different pitch and rotation speed have been disclosed by NASA.

2. Rotor Aerodynamic Simulation Method

2.1. Solving Equations. The Reynolds average Navier–Stokes (N-S) equation [15, 16] is used for solving:

$$\frac{\partial}{\partial t}\iiint_V \vec{W}\,dV + \iint_S \left(\vec{F}_c - \vec{F}_v\right)\cdot\vec{n}\,dS = 0, \tag{1}$$

where $\vec{W} = [\rho, \rho u, \rho v, \rho w, \rho e]^T$ is the conservation variable, $\vec{F}_c = (f, g, h)$ is the convection flux, and $\vec{F}_v = (a, b, c)$ is the viscous flux. They can be expressed as follows:

$$f = \begin{bmatrix} \rho u \\ \rho u^2 + p \\ \rho uv \\ \rho uw \\ \rho ue + up \end{bmatrix},$$

$$g = \begin{bmatrix} \rho v \\ \rho uv \\ \rho v^2 + p \\ \rho vw \\ \rho ve + vp \end{bmatrix},$$

$$h = \begin{bmatrix} \rho w \\ \rho uw \\ \rho vw \\ \rho w^2 + p \\ \rho we + wp \end{bmatrix},$$

$$a = \begin{bmatrix} 0 \\ \tau_{xx} \\ \tau_{yx} \\ \tau_{zx} \\ u\tau_{xx} + v\tau_{yx} + w\tau_{zx} - q_x \end{bmatrix},$$

$$b = \begin{bmatrix} 0 \\ \tau_{xy} \\ \tau_{yy} \\ \tau_{zy} \\ u\tau_{xy} + v\tau_{yy} + w\tau_{zy} - q_y \end{bmatrix},$$

$$c = \begin{bmatrix} 0 \\ \tau_{xz} \\ \tau_{yz} \\ \tau_{zz} \\ u\tau_{xz} + v\tau_{yz} + w\tau_{zz} - q_z \end{bmatrix}, \tag{2}$$

where the stress is expressed by

$$\begin{aligned}
\tau_{xx} &= \frac{2}{3}\mu\left(2\frac{\partial u}{\partial x} - \frac{\partial v}{\partial y} - \frac{\partial w}{\partial z}\right),\\
\tau_{xy} &= \tau_{yx} = \mu\left(\frac{\partial v}{\partial x} + \frac{\partial u}{\partial y}\right),\\
q_x &= -\mathrm{K}\frac{\partial T}{\partial x},\\
\tau_{yy} &= \frac{2}{3}\mu\left(2\frac{\partial v}{\partial y} - \frac{\partial u}{\partial x} - \frac{\partial w}{\partial z}\right),\\
\tau_{yz} &= \tau_{zy} = \mu\left(\frac{\partial w}{\partial y} + \frac{\partial v}{\partial z}\right),\\
q_y &= -\mathrm{K}\frac{\partial T}{\partial y},\\
\tau_{zz} &= \frac{2}{3}\mu\left(2\frac{\partial w}{\partial z} - \frac{\partial u}{\partial x} - \frac{\partial v}{\partial y}\right),\\
\tau_{xz} &= \tau_{zx} = \mu\left(\frac{\partial w}{\partial x} + \frac{\partial u}{\partial z}\right),\\
q_z &= -\mathrm{K}\frac{\partial T}{\partial z}.
\end{aligned} \tag{3}$$

The correlation between pressure and temperature is expressed by the following formula:

$$\begin{aligned}
p &= \rho(\gamma - 1)\left[e - \frac{1}{2}\left(u^2 + v^2 + w^2\right)\right],\\
p &= \rho RT,
\end{aligned} \tag{4}$$

where ρ is the density, p is the pressure, e is the total energy of gas per unit mass, μ is the viscosity coefficient, K is the heat conduction coefficient, T is the temperature, q_x, q_y, and q_z are the components of the heat flow along three directions, γ is the specific heat capacity, for ideal gas, $\gamma = 1.4$, and $R = 287.3$.

This study adopts the Spalart–Allmaras (S-A) turbulence model proposed by Spalart and Allmaras [17] because this turbulence model is widely used in the field of aerodynamic simulation of aircraft and has been verified by many cases.

The flow field of rotor is discretized by the finite volume method. According to different discrete methods of inviscid flux, different interpolation schemes are formed. In this study, Roe format [18] is adopted, which is a relatively common type of upwind format.

In the transient simulation of this study, the time discretization method adopts the dual time stepping method. Jameson [19] explained the principle and advantages of this method in his article.

The outermost boundary of helicopter flow field is set as nonreflective boundary, and the surfaces of rotor blades are set as nonsliding wall.

2.2. Grid System. The rotor motion is modeled by the embedded grid method. This method divides the flow field into multiple subdomains and generates mesh blocks for each subdomain. Different mesh blocks can be overlapped, nested, or covered.

For the aerodynamic simulation of helicopter rotor in this study, a structured embedded grid method is adopted. It is mainly composed of two parts. The first is an H-O grid surrounding the blades. In order to make the calculation results more accurate, the grid points in the area with significant viscous effect are locally encrypted. The H-O grid moves with the blade. The second is a stationary background grid nested on the H-O grid, which is a cylindrical region with a radius of $5R$. Its upper boundary is $3R$ away from the paddle plane, and its lower boundary is $5R$ away from the paddle plane, where R is the radius of the blade. Figure 1 shows the embedded grid system of helicopter rotor aerodynamic simulation in this paper.

3. Optimization of Hover Performance

The power load of the helicopter rotor in hovering conditions is mainly affected by the rotation speed, total pitch, radius, torsion angle, chord length, and other factors of the blades. Meanwhile, different airfoils also have certain influences on the power load of the rotor.

The power load formula of the rotor is shown as

$$q = \frac{G}{N_e^{(0)}}, \tag{5}$$

where q represents the gravity that the engine can lift at the rated power under standard atmospheric conditions at sea level, and its unit is N/kW. The gravity of the helicopter in hover is close to the pulling force of the rotor ($T \approx G$), and the output shaft power of the engine at sea level is simplified to the available power of the rotor ($(N_e^{(0)} \approx M * \Omega)$). M represents the torque of the rotor around the spindle, and Ω represents the angular velocity of the rotor.

The main purpose of hover performance optimization is to increase the power load of the rotor as much as possible on the premise of satisfying the limitation factors such as material strength and space. The higher the power load is, the less power the rotor needs to provide the same pulling force and the longer the helicopter's endurance is.

In the process of blade design and optimization, in order to ensure that the pulling force provided by the rotor is not changed, with the change of blade radius, total pitch, torsion angle, chord length, etc., the rotation speed of the blade should also be changed accordingly, resulting in different power loads of different blade models.

In this study, a method to optimize the hovering performance of helicopter rotors is designed. The specific steps are as follows:

(1) Determine the pulling force of the helicopter rotor designed in hover, defined as T_{desire}.

(2) Design an initial blade with a fixed aspect ratio and no torsion, and determine the number of blades, so as to obtain the initial rotor.

(3) An assumed total distance φ was given to the blade. Meanwhile, a relatively large rotation speed n_1 and a relatively small rotation speed n_2 were set, respectively. CFD method was used to calculate the rotor's pulling force T_1, T_2, and torque M_1 and M_2, respectively, at the rotation speed n_1 and n_2, which met the requirements of $T_1 > T_{\text{desire}} > T_2$.

(4) According to the formula $n_3 = n_1 - (T_1 - T_{\text{desire}}/T_1 - T_2) * (n_1 - n_2)$, the new rotation speed n_3 can be obtained. The CFD method was used to calculate the pulling force T_3 and torque M_3 of the rotor at rotation speed n_3. If $|T_3 - T_{\text{desire}}| < \varepsilon$, it is considered that the requirement of design hover tension can be met at the rotation speed of n_3. If $|T_3 - T_{\text{desire}}| \geq \varepsilon$, the formula $n_4 = n_3 - (T_3 - T_{\text{desire}}/T_3 - T_2) * (n_3 - n_2)$ is used to get the new rotation speed of n_4, and the CFD method is used again to calculate the pulling force T_4 and torque M_4 of the rotor at the rotation speed of n_4. In this way, iterate i times until $|T_i - T_{\text{desire}}| < \varepsilon$ is satisfied, which means that the design hovering pulling force requirement is satisfied when the rotation speed is n_i. The CFD method is used to calculate the pulling force T_i and moment M_i of the rotor at the speed n_i, and the power load q of the rotor can be obtained according to the rotation speed n_i, pulling force T_i, and moment M_i. Here, ε represents a small value, which is taken as 10 N in this paper.

(5) Given different total pitch of the blades, repeat steps 3 and 4 in turn to get the power load of the rotor at different total pitch, select the maximum power load, and take the total pitch corresponding to the maximum value as the optimal total pitch.

(6) The blades with the optimal total pitch were enlarged or reduced in turn according to the specified multiple, and then, steps 3 and 4 were repeated to calculate the power load of the models with different amplification or reduction multiples. On the premise that the strength, space, and other factors of the blade meet the design requirements, the radius of maximum power load is selected as the optimal radius of the blades.

(7) The blades with the optimal total pitch and the optimal radius were used to repeat steps 3 and 4 with different torsion angle successively, and the power loads of the blade models with different torsion angle were calculated. The torsion angle corresponding to the maximum power load was taken as the optimal torsion angle of the blades. In this study, the torsion angle of the designed blades changes according to the linear law.

(8) The blade models with the optimal total pitch, optimal radius, and optimal torsion angle were scaled to change the chord length, and steps 3 and 4 were repeated to obtain the power load of the blade models with different chord lengths. The chord length with the maximum power load is selected as the optimal chord length of the blades.

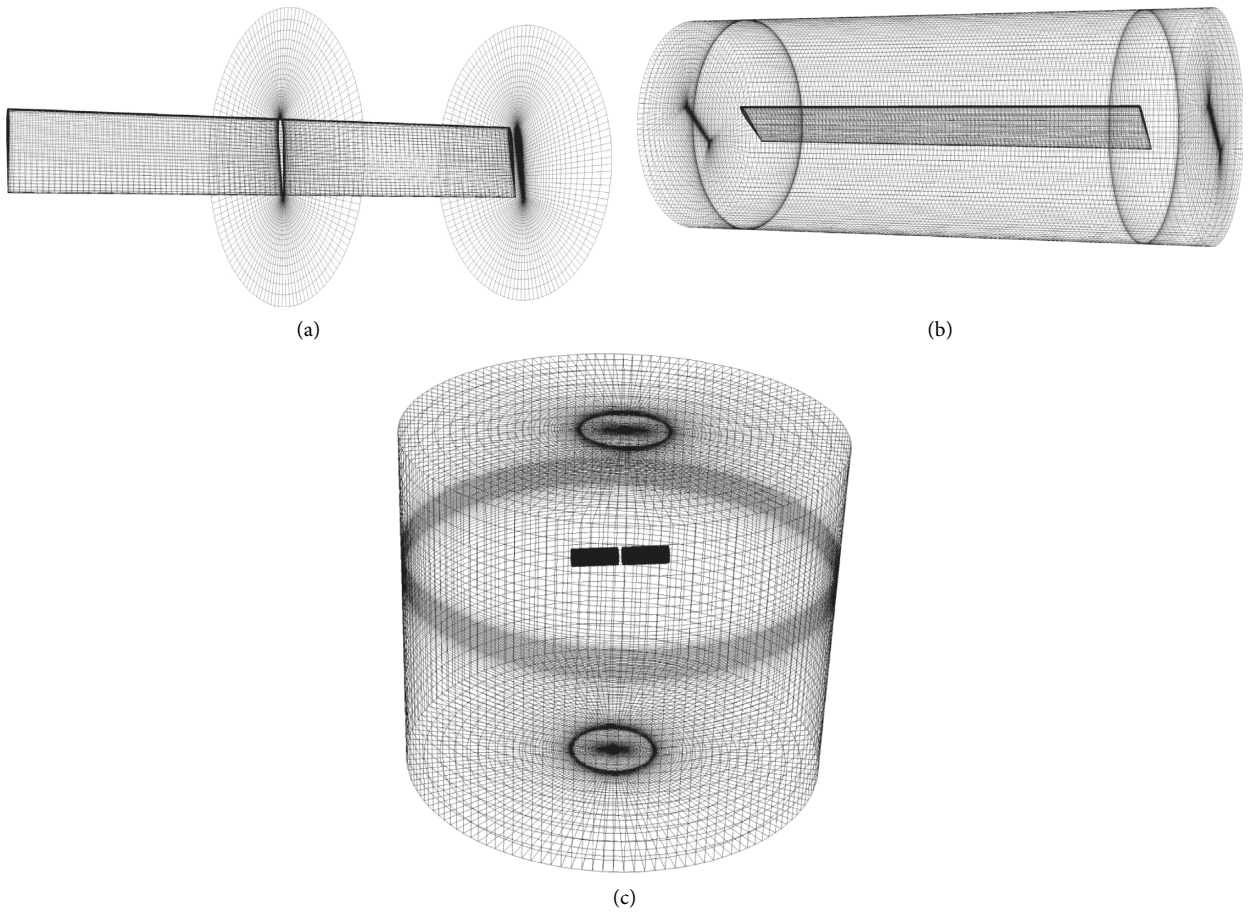

Figure 1: Embedded grid system of helicopter rotor aerodynamic simulation. (a) Profile of the blade grid. (b) An H-O grid around the blade. (c) Assembly of the embedded grid.

Table 1: Detailed design data of C-T rotor.

Number of blades (N)	2
Blade radius (R)	1.143 m
Plane shape of blade	Rectangle
Airfoil	NACA0012
Chord length (c)	0.1905 m
Undercut (R_{cut})	0.243R
Torsion angle	0°

By this method, the optimal parameters of the helicopter blade model can be obtained at a relatively low cost with only a few flight tests at the initial stage of blade design, thus greatly shortening the design cycle of the blade and saving a lot of research costs.

4. Examples and Discussion

In this study, taking the C-T [20] single rotor model as an example, the influence of blade radius, total pitch, torsion angle, and chord length on the power load of the rotor in hover is sequentially analyzed by the CFD method. Table 1 shows the detailed design data of C-T rotor.

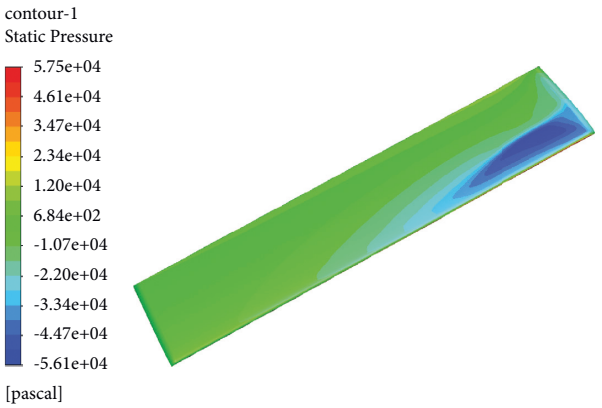

Figure 2: Pressure contours of C-T blade.

Four experimental states from NASA's experimental reports were selected to verify the credibility of the CFD method proposed in this paper. They are, respectively, (1) $M_{tip} = 0.433$, $\theta_c = 5^\circ$, $\Omega = 1250$ rpm, and $C_T = 0.00213$; (2) $M_{tip} = 0.612$, $\theta_c = 8^\circ$, $\Omega = 1750$ rpm, and $C_T = 0.00455$; (3) $M_{tip} = 0.877$, $\theta_c = 8^\circ$, $\Omega = 2500$ rpm, and $C_T = 0.00473$; (4) $M_{tip} = 0.612$, $\theta_c = 12^\circ$, $\Omega = 1750$ rpm, and $C_T = 0.00807$,

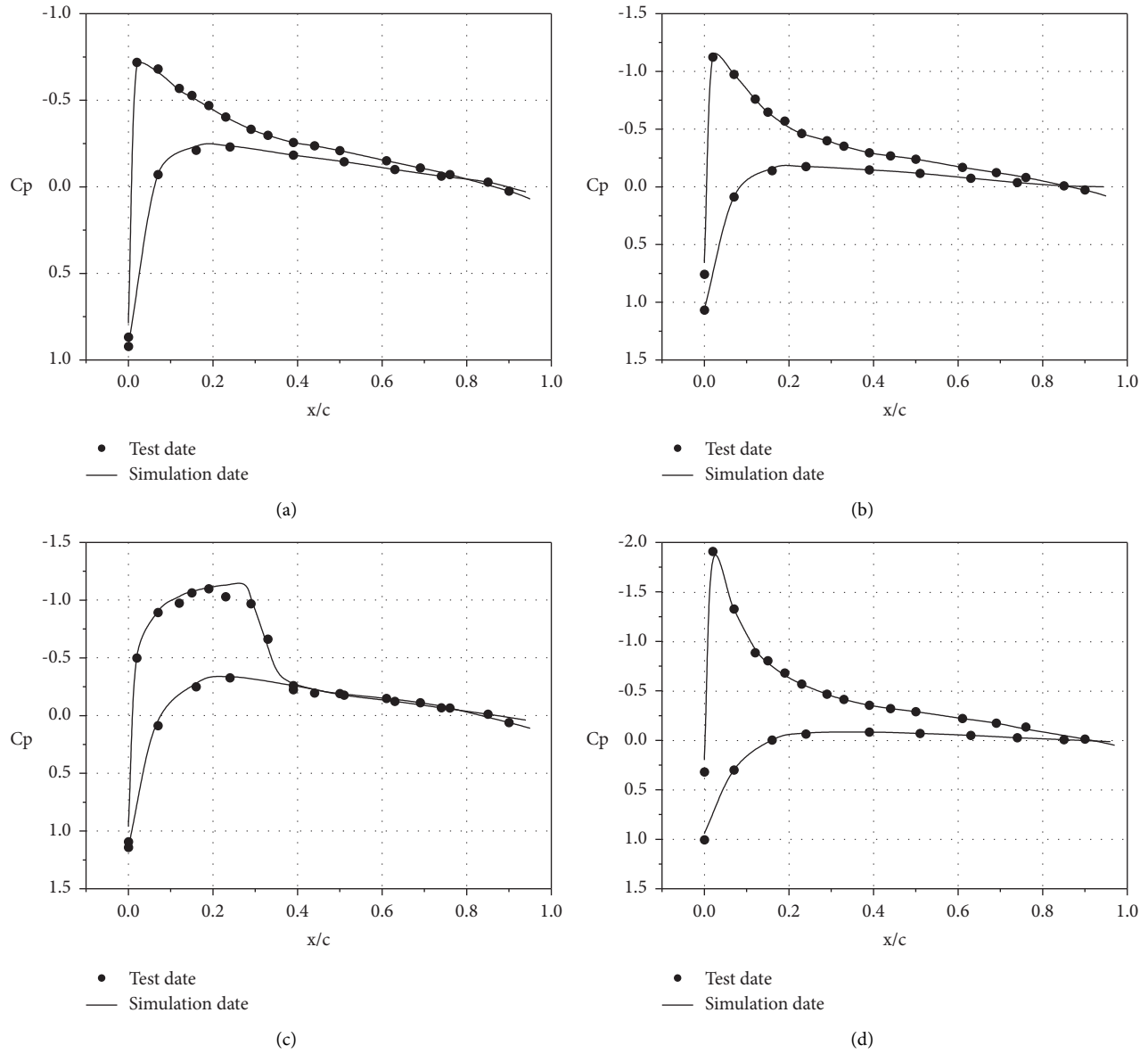

Figure 3: Surface pressure coefficients of C-T rotor at 0.96R profile in hover. (a) $M_{\text{tip}} = 0.433$ and $\theta_c = 5^\circ$. (b) $M_{\text{tip}} = 0.612$ and $\theta_c = 8^\circ$. (c) $M_{\text{tip}} = 0.877$ and $\theta_c = 8^\circ$. (d) $M_{\text{tip}} = 0.612$ and $\theta_c = 12^\circ$.

where M_{tip} is the Mach number at the blade tip, θ_c is the total pitch, Ω is the rotation speed, and C_T is the thrust coefficient of the rotor.

Figure 2 is the pressure contours of C-T rotor corresponding to test state 3. In this figure, obvious shock waves appear at the blade tip position of CT rotor.

Figure 3 compares the simulation date and the test date of the pressure coefficient at 0.96 R of the C-T rotor, from which it is not difficult to find that the simulation date and the test date are highly consistent.

Figure 4 shows the comparison between the simulation date and the test date of the thrust coefficient:

In Figure 4, SMA stands for simple moving average, which allows curves to appear in a smoother manner. The SMA formula is as follows:

$$\text{SMA} = \frac{x_M + x_{M-1} + x_{M-2} + \cdots + x_{M-(n-1)}}{n}. \tag{6}$$

Figure 4 shows that the simulation value of thrust coefficient is in good agreement with the experimental value.

In this study, working condition 3 is selected as the basic working condition before rotor performance optimization. Under this working condition, the thrust and torque of the rotor are 2218 N and 298.98 N $*$ m, respectively, by CFD calculation.

Firstly, the performance of the rotor was optimized by changing the total pitch of the blade. In the optimization process, the thrust value of the rotor calculated in working condition 3 was taken as the desired thrust T_{desire} of the rotor in hover. The thrust value calculated with a different total pitch should be almost equal, which is mainly realized by

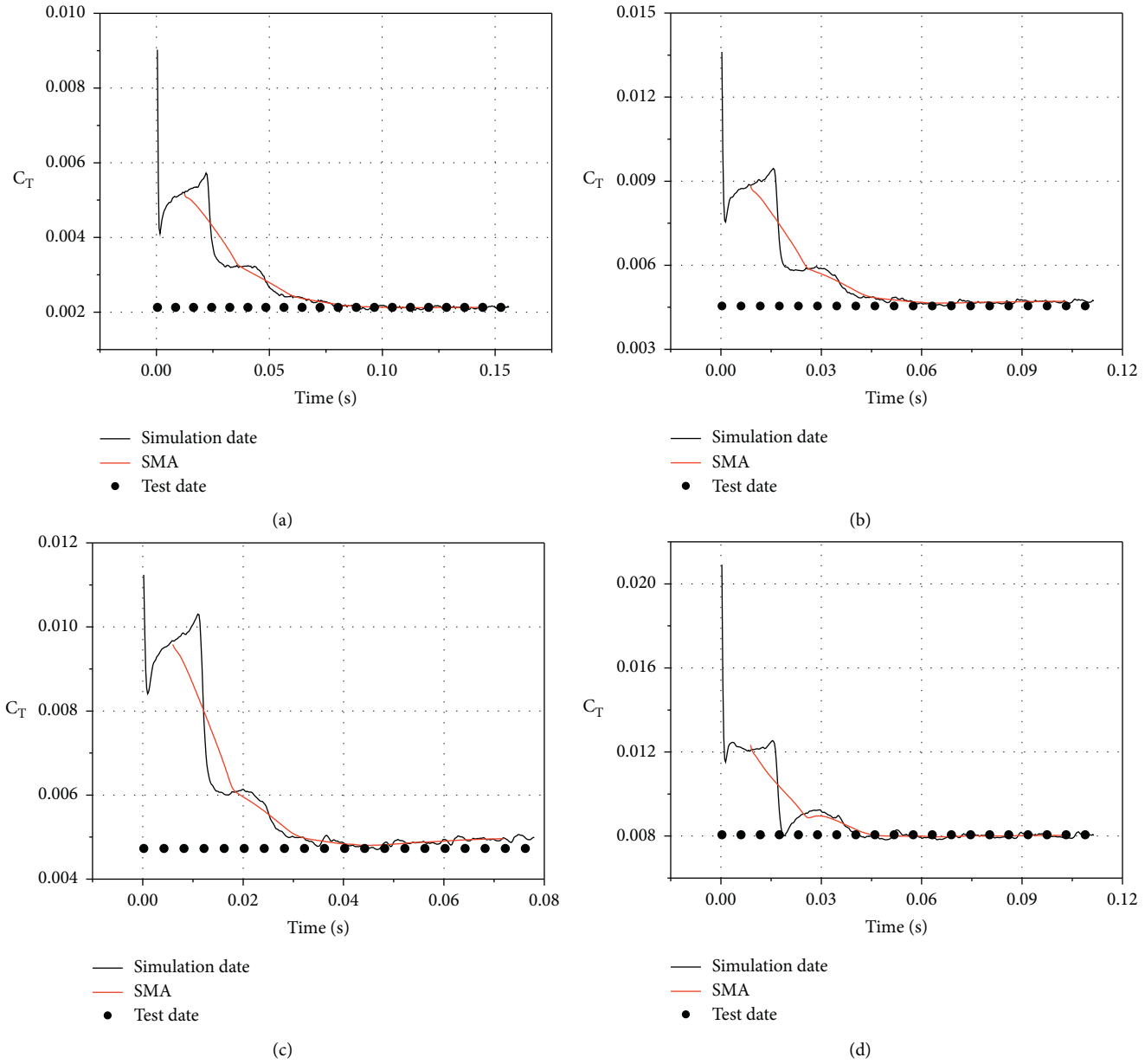

Figure 4: The comparison between simulation date and test date of thrust coefficient. (a) $M_{tip} = 0.433$ and $\theta_c = 5^\circ$. (b) $M_{tip} = 0.612$ and $\theta_c = 8^\circ$. (c) $M_{tip} = 0.877$ and $\theta_c = 8^\circ$. (d) $M_{tip} = 0.612$ and $\theta_c = 12^\circ$.

Table 2: CFD simulation results of rotors with a different total pitch.

Total pitch (°)	Rotation speed (rpm)	Thrust (N)	Torque (N ∗ m)	Power load (N/kW)
6	2975	2223	410.68	17.37
7	2730	2216	317.44	24.42
8	2500	2218	292.98	28.92
9	2320	2221	293.16	31.18
10	2180	2220	309.57	31.42
11	2060	2216	328.22	31.30
12	1962	2220	350.10	30.87
13	1890	2225	373.01	30.14
14	1825	2222	999.90	29.08

Table 3: CFD simulation results of rotors with different radius.

Radius (m)	Rotation speed (rpm)	Thrust (N)	Torque (N ∗ m)	Power load (N/kW)
0.8R	3310	2221	283.18	22.63
0.85R	2960	2219	281.82	25.40
0.9R	2660	2219	285.32	27.92
0.95R	2400	2212	294.58	29.88
R	2180	2220	309.57	31.42
1.05R	1977	2220	323.93	33.10
1.1R	1813	2220	336.44	34.75
1.15R	1660	2211	349.54	36.39
1.2R	1530	2212	367.92	37.52
1.25R	1415	2223	384.42	39.03
1.3R	1310	2222	400.71	40.43

Table 4: CFD simulation results of rotors with different torsion angles.

Torsion angle (°)	Rotation speed (rpm)	Thrust (N)	Torque (N ∗ m)	Power load (N/kW)
−2	1880	2226	323.24	34.97
−4	1890	2217	317.66	35.27
−6	1907	2218	314.88	35.28
−8	1920	2214	309.06	35.64
−10	1935	2221	306.05	35.82
−12	1950	2212	302.13	35.86
−14	1975	2219	302.86	35.42
−16	1995	2219	302.72	35.09

Table 5: CFD simulation results of rotors with different chord lengths.

Chord length (m)	Rotation speed (rpm)	Thrust (N)	Torque (N ∗ m)	Power load (N/kW)
0.8 ∗ 1.1c	2055	2216	292.57	35.20
0.9 ∗ 1.1c	2020	2228	297.09	35.45
1.0 ∗ 1.1c	1950	2221	302.13	36.00
1.1 ∗ 1.1c	1880	2222	310.82	36.31
1.2 ∗ 1.1c	1820	2215	317.32	36.62
1.3 ∗ 1.1c	1776	2219	318.47	37.46
1.4 ∗ 1.1c	1745	2220	320.28	37.93

changing the rotation speed of the rotor. Table 2 shows the results of CFD calculation:

It can be seen from Table 2 that when the total pitch is 10°, the C-T rotor has the maximum power load, that is, the optimal hovering performance. Therefore, the total pitch of 10° is selected as the optimal total distance of the blade.

The total pitch of the blades was maintained at 10°, and the airfoil, undercut, and aspect ratio remained unchanged. Then, the model of the blades was scaled up or down in equal proportion. Table 3 shows the results of the CFD simulation:

According to the analysis of Table 3, as the rotor radius increases, so does the power load of the rotor. Therefore, in theory, the blade radius should be as large as possible. However, due to the limitation of the blade material, if the radius of the blade is too large, it is easy to break. At the same time, the large-sized rotor is more likely to achieve large torque, which the engine cannot withstand. Considering comprehensively, 1.1R is temporarily selected as the optimal radius of the blade in this study, where R is 1.143 m. In the process of engineering design, the radius of the blade must be determined according to the rated parameters of the engine, so as to achieve a higher matching degree between the blade and the engine.

After the optimal size of the rotor radius is determined, the rotor blades are given different torsion angles, and the influence of torsion angle on the hovering performance of the rotor is analyzed through CFD simulation. The simulation results are shown in Table 4.

It can be seen from Table 4 that the rotor has the highest power load when the torsion angle is −12°, that is, the rotor has the optimal hovering performance. Therefore, −12° is chosen as the optimal torsion angle of the blades.

After the optimal values of the rotor's total pitch, radius, and torsion angle are selected, the power loads of the blades with different chord lengths are calculated to select the optimal chord length of blades. When determining the optimal radius of the blades, the proportion of the blades is enlarged by 1.1 times. Therefore, when selecting the blades with a radius of 1.1R as the basic model for the optimization analysis of chord length, the initial chord length should be 1.1c, and c is the chord length of the C-T rotor. The calculated results are shown in Table 5:

Table 5 shows that, for this design condition, the power load of the rotor increases gradually with the increase of chord length. However, bigger is not always better because too large a chord length can affect the forward flight performance of a rotor. In the process of engineering design, the determination of the chord length of the blades should also consider the requirements of working conditions such as forward flight of the helicopter.

Through the analysis in Tables 2 to 5, the optimal total pitch, optimal radius, optimal torsion angle, and optimal chord length of the rotor in hover can be determined in turn, thus obtaining an initial design scheme of the blade with excellent hovering performance.

5. Conclusion

This study proposes and verifies a CFD simulation method to optimize the hovering performance of helicopter rotors, from which some useful inspiration can be obtained:

(1) In this simulation, the Navier–Stokes equation is solved by the embedded grid method, and multiple working conditions of C-T rotor are calculated and verified, thus proving that the numerical method has high accuracy for rotor flow field in hovering state.

(2) Take the C-T rotor as an example to explain the optimization process in detail. This method avoids the shortcomings of traditional test methods, such as long research period and huge cost, and has high versatility. Therefore, it has the high engineering application value.

(3) There is still room for further improvement. In this study, the optimal value of each parameter is determined in order of total pitch, radius, torsion angle, and chord length. In the next step, we can try to exchange the order of each parameter to determine the optimal parameter order. In addition, the variation of chord length with radius should also be considered.

(4) The airfoil of the blade optimization example discussed in this study is NACA0012. In the engineering design stage, the blades of different airfoils should be optimized and compared, respectively.

(5) The CFD method does not consider the influence of blade deformation. In the next step, the coupling method of CFD/CSD can be adopted to fully consider the interaction between blade structure and flow field, so as to further improve the accuracy of simulation.

Data Availability

All data, models, and code generated or used during the study are included within the article.

Disclosure

Chenglong Zhou and Anan Xu are co-first author.

Conflicts of Interest

The authors declared no potential conflicts of interest with respect to the research, authorship, and/or publication of this article.

Acknowledgments

This study was funded by the National Key Research and Development Project of China (no. 2021YFC3002101).

References

[1] M. Costes, T. Renaud, and B. Rodriguez, "Rotorcraft simulations: a challenge for CFD," *International Journal of Computational Fluid Dynamics*, vol. 26, no. 6-8, pp. 383–405, 2012.

[2] C. L. Burley, T. F. Brooks, K. Y. Rozier et al., "Rotor wake vortex definition-evaluation of 3-C PIV results of the HART-II study," *International Journal of Aeroacoustics*, vol. 5, no. 1, pp. 1–38, 2006.

[3] N. M. Komerath, M. J. Smith, and C. Tung, "A review of rotor wake physics and modeling," *Journal of the American Helicopter Society*, vol. 56, no. 2, p. 22006, 2011.

[4] A. Brocklehurst and G. N. Barakos, "A review of helicopter rotor blade tip shapes," *Progress in Aerospace Sciences*, vol. 56, no. JAN, pp. 35–74, 2013.

[5] F. E. Tejero, P. Doerffer, and O. Szulc, "Numerical simula-tion of the tip aerodynamics and acoustics test," *Journal of Thermal Science*, no. 2, pp. 153–160, 2016.

[6] J. A. Benek, P. G. Buning, and J. L. Steger, "A 3-D chimera grid embedding technique," *7th Computational Physics Con-ference*, pp. 322–331, 1985.

[7] R. Steijl and G. Barakos, "Sliding mesh algorithm for CFD analysis of helicopter rotor-fuselage aerodynamics," *International Journal for Numerical Methods in Fluids*, vol. 58, no. 5, pp. 527–549, 2008.

[8] A. M. Wissink, M. Potsdam, V. Sankaran, and J. Sitaraman, "A coupled unstructured-adaptive Cartesian CFD approach for hover prediction," *66th Annual Forum Proceedings - AHS International*, pp. 1300–1317, 2010.

[9] J. Lim, A. M. Wissink, and B. Jayaraman, "Application of adaptive mesh refinement technique in Helios to blade-vortex interaction loading and rotor wakes," *67th American Helicopter Society International Annual Forum*, pp. 228–250, 2011.

[10] A. Jameson and D. Mavriplis, "Finite volume solution of the two-dimensional Euler equations on a regular triangular mesh," *AIAA Journal*, vol. 24, no. 4, pp. 611–618, 1986.

[11] Q. Zhao, G. Zhao, B. Wang, Q. Wang, Y. Shi, and G. Xu, "Robust Navier-Stokes method for predicting unsteady flowfield and aerodynamic characteristics of helicopter rotor," *Chinese Journal of Aeronautics*, vol. 31, no. 2, pp. 214–224, 2018.

[12] C. Zhou and M. Chen, "Computational fluid dynamics trimming of helicopter rotor in forward flight," *Advances in Mechanical Engineering*, vol. 12, no. 5, pp. 168781402092525–13, 2020.

[13] G. N. Barakos, T. Fitzgibbon, A. N. Kusyumov, and S. A. Jusyumov, "CFD simulation of helicopter rotor flow based on unsteady actuator disk model," *Chinese Journal of Aeronautics*, vol. 33, no. 09, pp. 37–52, 2020.

[14] W. Lyu, S. Wang, and A. Yang, "Some improvements of hybrid trim method for a helicopter rotor in forward flight,"

Aerospace Science and Technology, vol. 113, no. 9, p. 106709, 2021.

[15] G. X. Xiang, Y. C. Zhang, C. F. Zhang, and Y. Kou, "Study on initiation mechanism of oblique detonation induced by blunt bump on wedge surface," *Fuel*, vol. 323, p. 124314, 2022.

[16] G. X. Xiang, Y. Zhang, X. Gao, H. Li, and X. Huang, "Oblique detonation waves induced by two symmetrical wedges in hydrogen-air mixtures," *Fuel*, vol. 295, p. 120615, 2021.

[17] P. R. Spalart and S. R. Allmaras, "A one-equation turbulence model for aerodynamic flows," *Recherche Aerospatiale*, vol. 1, no. 1, pp. 5–21, 1994.

[18] P. L. Roe, "Approximate riemann solvers, parameter vectors, and difference schemes," *Journal of Computational Physics*, vol. 135, no. 2, pp. 250–258, 1997.

[19] A. Jameson, "Time dependent calculations using multigrid, with applications to unsteady flows past airfoils and wings," *10th Computational Fluid Dynamics Confer-ence*, vol. 1991, p. 87686, 1991.

[20] F. X. Caradonna and C. Tung, "Experimental and analytical studies of a model helicopter rotor in hover," *Vertica*, vol. 5, no. 2, pp. 149–161, 1981.